# **Enhancing Elderly Mobility: A Sturdy, Two-Body Robot for Handlebar Placement in Any Location**

Roberto Bolli Jr. and H. Harry Asada<sup>1</sup>

Abstract—Grab bars have been widely used for assisting elderly people with mobility and providing support for daily activities. This work aims to expand the notion of grab bars beyond fixed installations by the use of a mobile robot that can place a handlebar at any point in space, to optimally support postural transitions. A survey of elderly people and care professionals indicated that such a device must be sturdy, providing secure support without sliding or tipping over, yet also have a compact footprint to be maneuverable within confined spaces. Here, we propose a novel two-body robot structure, consisting of two small-footprint mobile bases connected by a four bar linkage where handlebars are mounted. Each base measures only 29.2 cm wide, making the robot likely the slimmest ever developed for mobile postural assistance. Through kinematic analysis, it is shown that the two-body structure can bear the entire weight of a human body, meeting required load bearing specifications as a handlebar. A control plan is proposed that is generalizable to all robots with two nonholonomic mobile bases connected by a coupling mechanism. This consists of a leader-follower scheme, in which the bases are connected by a virtual spring, as well as various enhancements to waypoint tracking and dead reckoning that allow the robot to smoothly and accurately follow a series of waypoints. A prototype robot is constructed, and its performance is validated experimentally. Index Terms—Physically Assistive Devices, Domestic Robotics, Nonholonomic Mechanisms and Systems.

# I. INTRODUCTION

The rapid increase in the elderly population, driven primarily by higher life expectancies and declining birth rates, has ushered in a myriad of challenges [1], [2]. One of the most prominent is the shortage of caregivers capable of delivering high-quality care to the aging population. In the U.S., approximately 800,000 elderly people are on waiting lists for subsidized care due to a lack of available workers [3]. Yet the caregiver shortage is only expected to become worse over the next decade, as more than 700,000 openings for caregivers are projected for each upcoming year, translating to a 25% increase from 2021 to 2031 [4]. Along with other factors, this has led to persistent sub-quality care for seniors, which prompted the White House to issue an executive order on April 18, 2023 to "improve support for caregivers ... and provide more care options for families [5]."

To address these concerns, many robotic devices have been proposed over the past two decades to augment the work of caregivers [6]. These range in function from social companions to item retrievers [7], health monitors, and mobility assistants [8]. Promising results have been reported

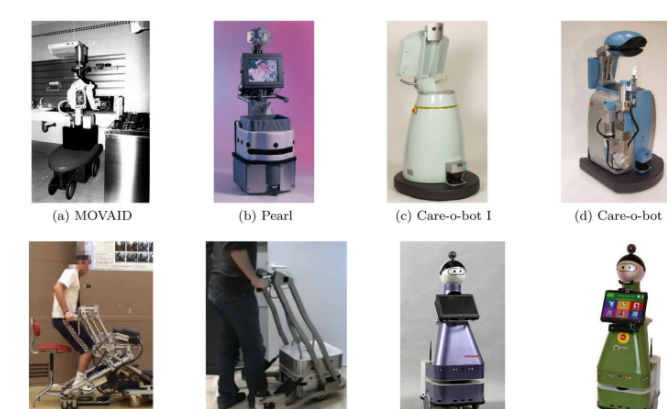


Fig. 1. An overview of eldercare mobility and service robots, adapted from [6]. Note the homogeneity in design: the robots' girth impedes their ability to navigate effectively through cluttered environments, and they cannot extend across obstacles such as the lip of a bathtub.

in enhancing the well-being of elderly people and decreasing the workload of their caregivers [7]. In particular, assistance with mobility is key to preserving the independence of older adults in daily activities. A few relevant eldercare robots are listed below.

Kompaï was equipped with a small handle to help the user stand up, as well as handlebars enabling use as a walker [9]. Robots such as MOVIAD and Pearl (Fig. 1a and b) were able to navigate a controlled household environment, and in the case of Pearl, to assist the user with ambulation. These three robots were limited in the sense that the handlebar was placed well within the robots' base of support, so the user needed to reach over and lean into the robot. RobuWalker (Fig. 1f) addressed this issue by the use of a U-shaped base, and was able to help the user perform a sit-to-stand transition [10]. Most other eldercare robots that assist with mobility have similar designs, consisting of either some sort of pedestal with a handlebar or essentially a mechanized walker (Fig. 1). While these prior works demonstrated efficacy in assisting elderly people, their use was generally limited to very specific scenarios, such as sit-to-stand transitions or ambulation. Applying high lateral forces could cause the pedestal to tip over. Lastly, the wide girth of some of the robots impeded effective navigation around obstacles.

To better assist users with multiple activities of daily living, we developed the Handle Anywhere (HA) mobile robot [11], whose utility lay in its ability to position a grab bar at any point in its workspace. Grab bars are commonly used postural support aids for elderly people and have been

<sup>&</sup>lt;sup>1</sup>Roberto Bolli Jr. and H. Harry Asada are with the Department of Mechanical Engineering at the Massachusetts Institute of Technology, 77 Massachusetts Ave., Cambridge, MA 02139, USA. rbolli@mit.edu, asada@mit.edu

shown to reduce the incidence of falls [12]. Oftentimes, however, the most beneficial room location to mount a grab bar for one motion (e.g. standing up in a bathtub) results in it becoming an obstacle for performing other motions (e.g. stepping out of the bathtub). The HA robot had the advantages of:

- Positioning the bar in a manner unconstrained by the room layout
- Offering support only when necessary, with the robot moving the handlebar to a new location after the motion had been completed

While the robot was able to successfully provide tele-assistance for postural transitions [11], its girth impeded navigation of cluttered home environments. In addition, the use of an off-the-shelf robot arm to position the handlebar significantly reduced the load bearing capacity. The U-shaped chassis was excellent for assisting with activities where the user could stand inside of the robot's base of support, but poor at providing support across distances such as a bathtub lip or coffee table. The wheels also slipped when high lateral force was applied, which is concerning because the robot's handlebar should ideally be as stable as a conventional grab bar.

In this paper, we present a novel robot for elderly assistance to address these limitations. Our robot, nicknamed the Two Buddy Bot (2BB) due to its two mobile bases, consists of a four-bar linkage spanning between two passively pivoting tread drive chassis. To the best of our knowledge, our kinematic design is unique to eldercare robots and perhaps even in the broader field of mobile robotics. This leads to distinct kinematic properties, including the challenges of navigation and motion control, which cannot be solved by continuous time-invariant stabilizing feedback [13].

The robot design is discussed in detail in section 2 and modeled mathematically in section 3. Section 4 explores the path following and control scheme as well as localization enhancements unique to this class of nonholonomic, linked tank drives. We assess the robot's ability to support activities of daily living and follow a trajectory in section 5. Finally, section 6 discusses the overall outlook of the robot system as an augmenter to caregivers in nursing homes, as well as proposed future work.

## II. MECHANICAL DESIGN

# A. Functional Requirements

We sought to tailor the robot's design to not only address the challenges of navigating a cluttered environment and extending over objects, but also to reflect the needs of elderly people. Accordingly, we initiated a user study with persons over the age of 65 to evaluate the difficulty of everyday tasks and preferred handlebar configurations [14], and browsed through previous studies of grab bars in seniors [15] [16]. Elderly people reported the most difficulty with getting out of a bathtub and reaching for items in drawers and cupboards, compared to other common activities of daily living [14].

Our first functional requirement is therefore that the robot must be capable of bearing up to the entire body weight of

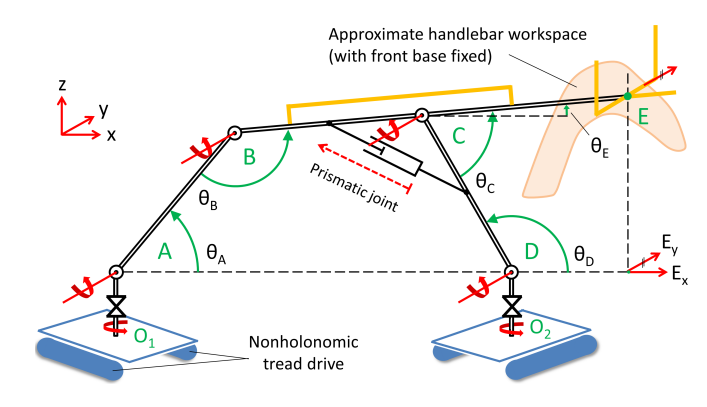


Fig. 2. Kinematic structure of the 2BB in the sagittal  $(E_x, z)$  plane.

an elderly user, since they may offload a significant amount of weight onto the handlebar while standing [15] or leaning down to grab an item. The robot should also be capable of omnidirectional motion to accommodate the small size of many bathrooms and the directional changes that occur when moving from one part of a bathroom to another [16]. The handlebar provided by the robot should be as stable as a grab bar secured to a wall, so the robot drive bases should have a high amount of traction, even on slippery and wet floors.

Furthermore, when asked to perform a sit-to-stand transition with a handlebar in the frontal (coronal) plane, the participants of the user study preferred the bar to be (on average,  $\pm$  1 standard deviation) 0.78  $\pm$  0.05 m off of the floor and  $0.61 \pm 0.09$  m away from their body [14]. The workspace of the robot must be able to accommodate these handlebar locations. We also noticed that elderly people commonly placed small tables and other objects in front of chairs. Therefore, the robot frame must be able to span over obstacles to assist in sit-to-stand transfers. The handlebar should be comfortable to grab and sized such that the elderly person can exert a power grip [17] as opposed to a pinch grip. Finally, the robot should be able to resist a high lateral force without tipping, as there is no guarantee that the user will only apply forces to the handlebars that are coaxial with the robot frame.

## B. Kinematic Structure

Consider a robot frame comprised of three links connected by revolute joints (Fig. 2). A virtual link between  $O_1$  and  $O_2$  turns the frame into a four-bar linkage. Links BC and CD are attached to a linear actuator which acts as an active prismatic joint. The linear actuator is not backdrivable and, thereby, joint C is rigidly fixed when not powered. This structure allows the handlebar (point E) to extend between 0.71 m and 1.37 m above the ground, meeting the workspace requirement in the previous section. The revolute joint on each end of the linkage (points A and D) is attached to a passive turntable. Each turntable connects via a zero-length link (e.g.  $\overline{AO_1} = 0$ ) to a nonholonomic drive base consisting of two parallel rubber treads.  $\theta_B$  and  $\theta_C$  are confined to remain below  $180^\circ$ , preventing the robot frame from entering any singularities. A long handrail is fixed to the top of the

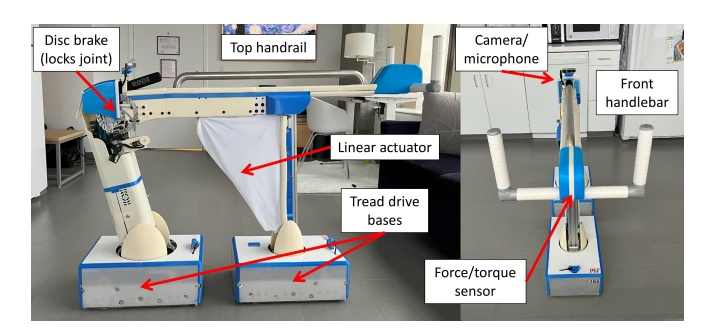


Fig. 3. Side view (left) and front view (right) of the 2BB with protective covers installed, shown in an apartment setting.

frame, and a triaxial handlebar (Fig. 2, point E) 3.2 cm in diameter is placed at the robot's endpoint. This allows the front handlebar to provide a comfortable power grip for the user from any orientation. Furthermore, the component of the handlebar coaxial with link BC is made to be magnetically retractable, so that when the user is facing the robot, he/she can grab the handlebar without being impeded.

This kinematic structure allows the front handlebar to move omnidirectionally in 3D space using only five actuators: one for each tread and one for the prismatic joint. While the robot system itself is nonholonomic, the passive turntables allow each drive base to rotate in place without displacing the handlebar, which enables the handlebar to be moved in any direction. The two body structure is advantageous for bearing the downward load and load coaxial to link BC, which are the dominant forces exerted during sagittal plane postural transitions such as sit-to-stand [18]. Additionally, the robot forms a virtual closed-loop chain with the ground, which aids in stability.

# C. Performance Metrics

Table 1 lists the relevant performance metrics of the prototype robot system shown in Fig. 3. The robot weight and frame dimensions were informed by static analysis of the maximum expected handlebar load (section 3A). Unique to this robot is its ability to support the full weight of a human located outside the base of support of the robot. To our knowledge, this is the only eldercare robot that can achieve such a task at large distances (up to 61 cm from the front base). Additionally, it is the narrowest eldercare robot designed for postural support in the literature at just 29 cm wide. This enables a person to walk alongside the robot in a narrow corridor while holding on to the top handlebar for assistance, and aids the robot in navigating between chairs, tables, and other objects. The frame span of 66 cm is wide enough to arch over a coffee table and help a user stand up from a couch or chair.

#### III. MODELING

# A. Statics

The necessary mass of the robot  $m_{robot}$  was determined by a torque balance based on a lateral pull strength of 120 N. The average pull strength of an adult male is 147.6 N

TABLE I
KEY DIMENSIONS AND PERFORMANCE METRICS

Dimension	Value	Notes
Base width	29.2 cm	Smaller values lead to high shear forces and tread slip during base rotation
Base length	47 cm	Constrained by length of tread
Link AB, BC, and CD	61 cm	
Top of frame length	1.2 m	Distance from B to E
Max / min handlebar height from ground	1.37 / 0.71 m	Encompasses full range of preferred handlebar locations in [14]
Max / min robot length (measured at ground level)	2.67 / 0.94 m	The back of the frame sometimes protrudes behind the rear base
Max handlebar span	61 cm	Ground distance from front base to point E; sufficient to extend into a tub or bed
Max frame span	66 cm	Distance from A to D
Robot weight	77 kg	More weight improves traction and increases resistance to tipping over
Max supported weight at front handlebar	100 kg	Dependent on robot configuration; more weight can be supported the farther apart the bases are located
Max axial force be- fore slippage	450 N	Dependent on ground surface; estimated on vinyl tile floor ( $\mu = 0.6$ )
Max lateral force be- fore tipping	120 N	Average max pull strength of an adult male is 147.6 N [19], and is much lower in elderly persons

[19], and is much lower in elderly persons due to muscle degeneration. Assuming the robot is in the configuration in Fig. 2, when  $F_{E_y}=120N$  is applied at the handlebar E along the  $\hat{E}_y$  direction, the ground reaction torque provided by the drive bases is dependent on the distance from the CoM of the robot to the side of each base,  $d_{\text{CoM to side}}$ . The robot is narrowest when both drive bases are parallel to the frame, as they are in Fig. 3, which means the minimum value of  $d_{\text{CoM to side}}=$  base width divided by 2=14.6 cm. Balancing the moments in the  $(E_y,z)$  plane, where g represents the acceleration due to gravity and  $\hat{z}$  is the z-axis unit vector,

$$m_{robot} g d_{\text{CoM to side}} - F_{E_y} \left( \overrightarrow{O_2 E} \cdot \hat{z} \right) = 0$$
 (1)

$$m_{robot} = rac{F_{E_y}\left(\overrightarrow{O_2E}\cdot\hat{z}
ight)}{q\,d_{\text{COM to side}}} = 75kg$$

It was discovered that placing a large downward force  $F_z$  and/or horizontal force  $F_{E_x}$  on the handlebar would cause the rear base to slide to its neutral position, where link AB is vertical. This is because any handlebar load in the  $(E_x,z)$  plane results in a force  $F_{AB}$  axial with link AB, due to the moment about the front base  $O_2$ .  $F_{AB}$  leads to a force  $F_{lateral}$  in the xy plane pulling the rear drive base along the ground, dependent on  $\theta_A$ .

$$F_{AB} = \frac{F_{E_x}(\overrightarrow{O_2E} \cdot \hat{z}) - F_z(\overrightarrow{O_2E} \cdot \hat{E}_x)}{\overrightarrow{O_2B}} \cdot \hat{\overrightarrow{AB}}$$
 (2)

$$|F_{lateral}| = F_{AB}\cos(\theta_A) \tag{3}$$

When  $|F_{lateral}|$  is small, friction with the ground prevents the rear base from slipping. Denoting the coefficient of

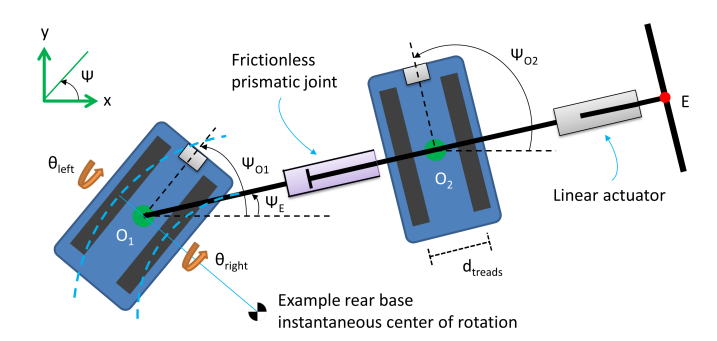


Fig. 4. Kinematic representation of the 2BB in the overhead plane. The four-bar frame linkage is modeled as a frictionless prismatic joint with a linear actuator between the handlebar and front base. The instantaneous center of rotation of each base is dependent on the velocity of each tread.

friction between the treads and the ground as  $\mu$ , the drive base will not slip as long as

$$|F_{lateral}| \le \mu \left( m_{base} g - F_{AB} \sin(\theta_A) \right)$$
 (4)

The mass of each base  $m_{base}$  is approximately 32 kg, and the coefficient of friction  $\mu$  is  $\geq 0.5$  on most floors (see section 5 for experimental measurements). When  $\theta_A=45^\circ$  as in Fig. 2, the rear base will slide such that link AB becomes vertical if the total downward and horizontal force on the handlebar  $(F_z+F_{E_x})$  exceeds around 200 N. To prevent this from occurring, a bicycle disc brake is used to selectively lock joint B (Fig. 3, left) when the front handlebar is grabbed. This effectively turns the three-bar frame into a single rigid body when the brake is active, ensuring that the distance between the bases  $\overline{O_1O_2}$  stays constant and the frame does not change configuration under an applied load.

The maximum vertical force  $F_z$  the handlebar can bear is dependent on the frame pose and if the brake on joint B is locked. Assuming it is, a moment balance about  $O_1$  (eq. 5) shows that  $F_z$  reaches high values as the ground distance between the handlebar and the front base approaches zero, that is,  $(\overline{O_2E}\cdot\hat{E}_x)\to 0$ . Here,  $\hat{E}_x$  represents the direction of link BE along the ground plane xy.  $(\overline{O_2E}\cdot\hat{E}_x)$  is shown in Fig. 2 as the dashed horizontal line between D and the projection of E onto the xy plane. The contribution of the weight of the frame to the moment is negligible and can be ignored. If the materials used to construct the frame are sufficiently strong, the theoretical maximum load bearing capacity approaches infinity as the handlebar moves over the front base, since  $\overline{O_2E}$  becomes zero. In the pose shown in Fig. 3, the robot can support around 75 kg.

$$|F_z| \le \frac{m_{base} \, \overline{O_1 O_2} \, g}{(\overline{O_2 E} \cdot \hat{E}_x)} \tag{5}$$

# B. Kinematics

Under the assumption that both bases stay in contact with the ground at all times, a virtual link connects joints A and D (dashed line in Fig. 2). This creates the following constraint equations for the robot frame, which can be solved to determine the pose of the frame using only one joint angle.

$$\theta_A + \theta_B + \theta_C + \theta_D = 2\pi \tag{6}$$

$$\overline{AB}\cos(\theta_A) + \overline{BE}\cos(\theta_A + \theta_B) = \overline{CD}\cos(\theta_D) + \overline{CE}\cos(\theta_D + \theta_C + \pi)$$
(7)

$$\overline{AB}\sin(\theta_A) + \overline{BC}\sin(\theta_A + \theta_B) + \\ \overline{CD}\sin(\theta_A + \theta_B - \theta_C) = 0$$
(8)

Because each drive base is nonholonomic, the current pose of one base can only be obtained by integrating the time history of the tread angles, or using forward kinematics if both the location of the other base and the angle of one of the frame joints ( $\theta_A$  through  $\theta_D$ ) is known. From here, standard kinematic techniques can be used to determine the location of the front handlebar. The rotation of the handlebar about  $\hat{E}_x$  (i.e. the pitch) will always be zero, since the kinematic couplings prevent the frame from tilting laterally. Therefore, the handlebar pose can be defined along 5 axes in 3D space.

$$p = [x_E, y_E, z_E, \theta_E, \Psi_E] \tag{9}$$

Despite the system being nonholonomic, there exist one, two, or four unique inverse kinematics solutions for a desired handlebar pose. This is due to the linkage attached to each base (AB and CD) taking one of two possible poses, mirrored about the z axis. If each of the angles  $\theta_B$  and  $\theta_C$  are  $\geq \pi/2$ , the same handlebar pose can be achieved by  $\pi - \theta_B$  and  $\pi - \theta_C$ , respectively. These configurations can be found analytically using the range of motion of each joint (specified in section 2B).

The Jacobian J of the robot system  $\dot{p}=J\dot{q}$  can be found by analyzing the robot in the overhead (x,y) and sagittal  $(E_x,z)$  planes, as shown in Fig. 2, with

$$\dot{q} = [\dot{\theta}_{O_1, \, left}, \, \dot{\theta}_{O_1, \, right}, \, \dot{\theta}_{O_2, \, left}, \, \dot{\theta}_{O_2, \, right}, \, \dot{\theta}_{C}]$$

where  $\dot{\theta}_{O_1,\,left}$  is the angular velocity of the left tread on the rear base. For each drive base b, the Jacobian relative to the global coordinate system is

$$\begin{pmatrix} \dot{x_b} \\ \dot{y_b} \\ \dot{\Psi_b} \end{pmatrix} = \begin{pmatrix} \frac{r_{\text{tread}}\cos(\Psi_b)}{2} & \frac{r_{\text{tread}}\cos(\Psi_b)}{2} \\ \frac{r_{\text{tread}}\sin(\Psi_b)}{2} & \frac{r_{\text{tread}}\sin(\Psi_b)}{2} \\ \frac{r_{\text{tread}}}{d_{\text{treads}}} & \frac{r_{\text{tread}}}{d_{\text{treads}}} \end{pmatrix} \begin{pmatrix} \dot{\theta}_{\text{right}} \\ \dot{\theta}_{\text{left}} \end{pmatrix}$$
(10)

where  $r_{treads}$  is the radius of each tread and  $d_{treads}$  is the distance between treads, as shown in Fig. 4. The back base,  $O_1$ , causes the endpoint E to rotate about  $O_2$ :

$$\begin{pmatrix} \dot{x}_E \\ \dot{y}_E \end{pmatrix} = \begin{pmatrix} \frac{\overline{O_2 E} \sin(\Psi_{O_1} - \Psi_E)}{\overline{O_1 O_2}} & 0 \\ 0 & \frac{\overline{O_2 E} \sin(\Psi_{O_1} - \Psi_E)}{\overline{O_1 O_2}} \end{pmatrix} \begin{pmatrix} \dot{x}_{O_1} \\ \dot{y}_{O_1} \end{pmatrix}$$
(11)

The front base  $O_2$  causes the endpoint E to extend radially and rotate around  $O_1$ . As in eq. 11, the transformation matrix between  $(\dot{x}_{O_2},\,\dot{y}_{O_2})$  and  $(\dot{x}_E,\,\dot{y}_E)$  is diagonal, with both non-zero elements equal to

$$\cos(\Psi_{O_2} - \Psi_E) \frac{(\overline{O_1 O_2} + \overline{O_2 E}) \sin(\Psi_{O_1} - \Psi_E)}{\overline{O_1 O_2}}$$
 (12)

From eq. 10, 11, and 12, we can obtain a Jacobian for the endpoint xy coordinates. The endpoint angle  $\dot{\Psi}_E$  is related

to each tread's velocity  $\dot{\theta}_{tread}$  by the following expression, which is multiplied by -1 for the rear base.

$$\dot{\Psi}_E = \frac{r_{\text{tread}} \sin \left(\Psi_E - \Psi_{\text{base}}\right)}{2 \overline{O_1 O_2}} \dot{\theta}_{base, tread}$$
 (13)

Forward kinematic equations relate points  $O_1$  and  $O_2$  to the endpoint height  $z_E$  and angle  $\theta_E$ . From here, the full robot Jacobian can be assembled. Numerical analysis found that it is rank deficient, with the rank degenerated to 3. Specifically, only two of the three 2D ground planar motion coordinates are independent, as is expected from a nonholonomic system, and the yaw of the handlebar  $(\Psi_E)$  is dependent entirely on the location of the bases.

#### IV. CONTROL SCHEME

Previous works [13], [20] have developed strategies for path planning, trajectory generation, and trajectory tracking for an active car/passive trailer system. However, only the lead car was powered, and the trailers were connected by passive revolute joints. Work has also been done on trailers that are actively steered [21] but have free spinning wheels. Our robot differs from these systems as each base is actively powered, the treads introduce significant slip, and the fourbar linkage connecting the bases acts as a passive prismatic joint (Fig. 4). Thus, new control methods are necessary, which are generalizable to all robots with two nonholonomic tread drives connected by a variable-length coupling.

Nonholonomic vehicles are frequently globally controllable when linearized about a nonstationary trajectory [22]. However, when the system is linearized about a certain pose, it is often not controllable, and there exists no continuous time invariant stabilizing feedback for driftless nonholonomic systems [23], [24]. Due to these difficulties, standard motion planning techniques for holonomic systems cannot be directly applied to nonholonomic motion [13]. We thus introduce a trajectory following scheme for the 2BB and several enhancements to dead reckoning.

# A. Path Generation and Trajectory Following

The robot is commanded to follow a series of waypoints via dead reckoning of the tread angles. For simplicity, the front base path is crafted manually (example path shown in Fig. 5). The final front and rear base poses are calculated kinematically based on a desired terminal handlebar pose.

A basic navigation method we call "point and shoot" involves rotating each base to align with the subsequent waypoint and then driving straight towards it. Although this approach is valid in geometric path tracking, the motion is jerky and disjointed, since the bases have to change between pure translation and pure rotation at each waypoint. Here, the goal is to develop a simple algorithm to minimize jerkiness while maintaining path fidelity. We achieve this by shifting the instantaneous center of rotation [25] (see Fig. 4) of each drive base.

- Sequential waypoints that are either duplicates or very close to each other are removed.
- 2) The first three waypoints are loaded into a segment.

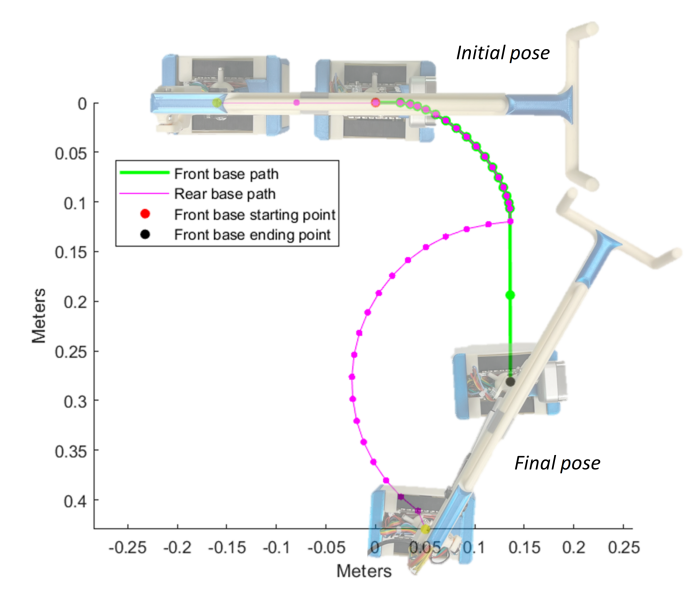


Fig. 5. Example path for the drive bases on a 1:4 scale model of the 2BB. The corresponding initial and final robot pose is overlaid onto the plot.

- 3) To find the segment's instantaneous center of rotation, a circle is fit to minimize the squared error. If the points are exactly or nearly linear, a circle of radius r = 1000 meters is used.
- 4) The base is rotated to be tangent to the circle.
- 5) The base is driven along the circle from the first to second waypoint.
- 6) Once the base reaches the second waypoint, steps 3-5 are repeated using a segment comprised of the second waypoint and the two successive waypoints, until the final waypoint is reached.

A dummy waypoint is added to the end of the trajectory since two lookahead points are always required (step 6). While the bases still rotate at each waypoint (step 4), the magnitude of rotation is less than the "point and shoot" method, since part of the rotation is accomplished through following the circular trajectory (step 5). Compared to conventional strategies such as pure pursuit [26], this scheme guarantees that the robot will hit every waypoint. Other reconfigurable robots [27], [28] have found success in modulating the center of rotation to follow a path, under different kinematic and vehicular constraints.

## B. Rear Base Coordination

The rear base is commanded to follow the same trajectory as the front base while remaining a nominal distance  $d_0$  behind, causing the robot to slither like a snake. While many alternative coordination strategies exist, this scheme is particularly useful for reducing the width of a path and thereby avoiding collisions with obstacles. Additionally, it is only required to design a single trajectory (the front base) as opposed to two trajectories for both mobile bases.

The maximum and minimum base separation, denoted as  $d_{min}$  and  $d_{max}$ , was calculated from the joints' physical range of motion (section 2B). At any point in the trajectory,

the frame is being either compressed or elongated by each base, unless the base is stationary or undergoing pure rotation about its centerpoint  $(O_1 \text{ or } O_2)$ . This results in a respective decrease or increase in d, the distance between the bases. The magnitude of compression or elongation is dependent on the translational velocity  $\vec{v}_{trans}$  of each base, which can be obtained using the vehicle Jacobian in eq. 10. We define an indicator variable  $\lambda_{base} = sign(\vec{v}_{trans} \cdot \hat{\Psi}_E)$ , where  $\hat{\Psi}_E = [\cos{(\Psi_E)}, \sin{(\Psi_E)}]$  in the xy plane. For the front base, if  $\lambda = 1$ , the base's velocity is increasing the distance d between bases, and if  $\lambda = -1$ , it is decreasing d. The reverse is true for the rear base. We modulate the speed of each base |v| to be linearly proportional to d, scaled by the base's target speed  $|v^0|$ .

If 
$$\lambda_{base} > 0$$
 and  $d > d_0, |v| = |v^0| \frac{d - d_0}{d_{max} - d_0}$   
If  $\lambda_{base} < 0$  and  $d < d_0, |v| = |v^0| \left(1 - \frac{d - d_0}{d_{min} - d_0}\right)$ 

This creates a virtual exponential spring on the distance between the two bases, since the rate of change of the base separation  $\dot{d}$  is proportional to d, resulting in a well of stability in the vicinity of  $d_0$ . Damping is introduced from friction within the robot system, making it very stable even at high stiffnesses. As d is measured directly using the absolute encoders on the frame joints, the control scheme is fully decoupled from the robot's trajectory unless both bases are commanded to drive towards or away from each other. In such cases, the robot will stop as it approaches  $d_{max}$  or  $d_{min}$ , since each base's velocity will be decreased to zero.

# C. Enhancements to Dead Reckoning

Sensor measurements of the angles of the revolute joints and turntables significantly increase the dead reckoning accuracy of each base. We can exploit kinematic constraints among these sensor readings for improved pose estimates. These strategies are unique to this type of robot. We leverage the fact that the treads only tend to slip if the bases are turning, but provide excellent traction when moving linearly. Precise modelling of the tread slippage, which is difficult due to undulations in the ground surface and the accumulation of debris on the treads, is not required.

- Base angle: When a drive base follows a relatively linear trajectory or remains stationary, implying a nearly constant angle (see Fig. 4), the angle of the other base is updated using the former base's estimated angle and the encoders on the turntables, which measure the base rotation relative to  $O_1E$ . For example,  $\Psi_{O_1} = \Psi_{O_2} \Psi_{O_2,O_1E} + \Psi_{O_1,O_1E}$
- Base position: In the same scenario, the position of one base and the measured frame pose is used to calculate the actual position of the other base. This helps to correct for slippage when the latter base is making a sharp turn. The next few waypoints (corresponding to a path distance of 0.6 m) are shifted by successively smaller intervals to redirect the base to the desired path.

In all other cases, the base position is updated using dead reckoning via tread encoder readings.

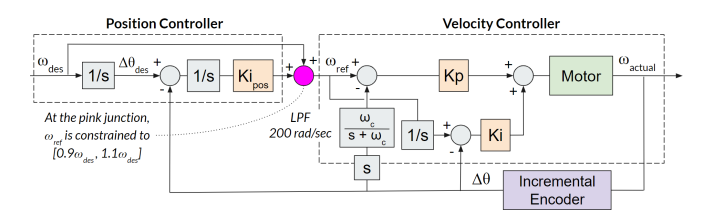


Fig. 6. Tread motor controller. The position controller helped to eliminate steady-state position error by increasing or decreasing the reference velocity by up to 10%. All integrators had anti-windup protection.

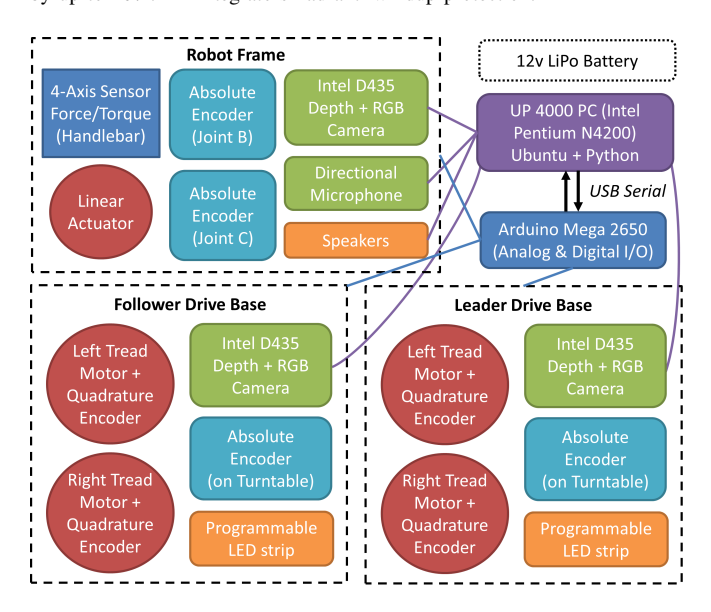


Fig. 7. Block diagram of the 2BB robot system.

#### D. Low-level Motor Control

Fig. 6 shows the control scheme for each motor, which consists of a proportional-integral velocity controller with a feedforward term and an integral position control outer loop. The position controller is nonlinearly constrained to saturate at  $\pm$  10% of the desired tread velocity, which helps to reduce steady-state position error (inherent to PI velocity control) while avoiding large deviations from the intended velocity. To prevent windup, the desired tread angle is reset every time the motor velocity is set to zero.

#### V. IMPLEMENTATION AND EXPERIMENTAL VALIDATION

Tight-tolerance turntables were used on each base to minimize lateral sway; this proved to be particularly necessary due to the amplification of sway from the bottom to top of the frame. The tread drive was constructed from a large rubber timing belt run through three cogs, with the center cog dropped by approximately 0.2 cm to ease shear force on the treads during base rotations. The coefficient of friction on common household floors was estimated to be  $\geq 0.6$  on dry linoleum, 0.5 on wet linoleum, and  $\geq 0.55$  on low-pile carpet, providing traction comparable to a car tire [29].

Absolute encoders were added to the revolute joints on the top frame link and to the base turntables, as shown in Fig. 7. Coupled with the kinematic constraints of the frame, this allowed the controller to assess the real-time pose

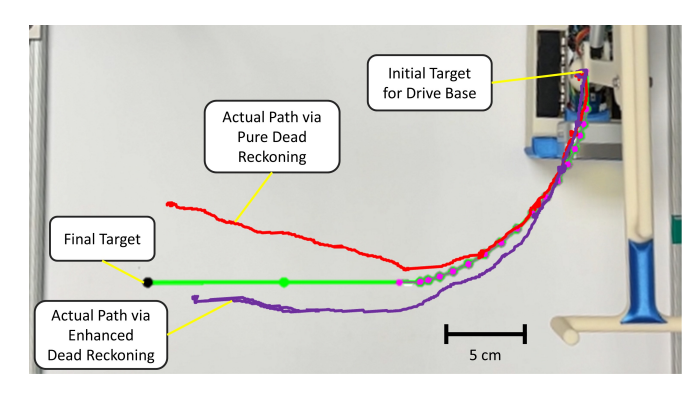


Fig. 8. Trajectory tracking performance of the front base of a 1:4 scale robot model. Shown is the desired path (green line), dead reckoning (red line), and dead reckoning plus the enhancements in section 4C (purple line).

of the robot relative to the handlebar. The handlebar was instrumented with a four-axis force/torque sensor created by assembling two 50 kg strain gauges perpendicular to each other, and attaching two such assemblies to the handlebar a fixed distance apart. Each tread on the drive base was equipped with a quadrature encoder for closed-loop control up to  $\approx 0.45$  m/s.

Consent is paramount in caregiving, so the robot was equipped with a directional microphone to capture audio in the vicinity of the handlebar as well as speakers for the teleoperator to speak with the user. To prevent collisions with a user's foot, each drive base was instrumented with a strip of LED lights that could change color depending on the base's motion. A trio of Intel D435 depth cameras were used for navigation; one on the top of the frame to map the room and additionally serve as an RGB camera for the teleoperator, and one on the front of each base to detect obstacles. Finally, the robot was padded with elderly-safe plastic and foam covers, and any potential pinch points were covered.

Fig. 8 shows the performance of the robot in tracking a simple trajectory. It is clear that the enhancements in section 4C significantly improved the tracking fidelity, decreasing the maximum path deviation by around 65%. In accordance with the treads' tendency to slip during turns, the largest improvement was visible by the end of the turn. The final positioning accuracy was 1.7x higher with the enhancements. The algorithm in section 4A decreased the amount of corrective rotation (step 4) by up to 60% compared to point and shoot, leading to smoother and more fluid motion.

#### A. Use Case Studies

The robot was successfully teleoperated, with each drive base mapped to a 2D joystick. The operator was able to learn to control the robot in a short amount of time (approx. 5 mins) and navigate between doorways, desks, and other obstacles. Common household scenarios were enacted with an adult subject to test the robot's physical and haptic support, shown in Fig. 9. These scenarios reflect the activities that elderly people have difficulty performing [14], especially getting out from a bathtub and reaching up or down for items, which were rated as the most challenging tasks around the



Fig. 9. Use cases: demonstration of the 2BB providing assistance with common activities of daily living. From left to right, the first row shows ambulation in a corridor, standing up in a bathtub, and stepping over a bathtub lip onto a slippery floor. Row 2 demonstrates standing up from a couch, using the robot as a walker, and sit-to-stand from a toilet. Row 3 demonstrates reaching up to grab an item from a shelf, and reaching down to grab an item from a drawer (shown from two different angles).

home [14]. In each situation, the robot was able to provide postural assistance as intended, and decreased the subject's perceived effort for performing the task. Additionally, the frame successfully spanned household objects such as a coffee table, and extended the handlebar over the lip of a bathtub. Five of nine elderly persons surveyed were open to using the robot in their home [14], suggesting a receptive market for adoption. The others didn't require home assistance or expressed concerns about reliability.

There was also a statistically significant decrease in the average time to perform a sit-to-stand transition when the elderly persons used a frontal handlebar at their preferred height (Fig. 10). The perceived difficulty on a scale of 1 to 5, with 1 being the easiest, decreased from 1.67  $\pm$  0.58 (1 standard deviation) to 1.0  $\pm$  0. Six out of eight elderly persons (75%) said that the handlebar made it easier for them to stand up, and the other 25% had no problem standing up without the handlebar.

# VI. CONCLUSION AND DISCUSSION

We have successfully developed an eldercare robot to assist with postural transitions around the home, with a novel form factor able to navigate obstacles and extend over objects. To our knowledge, this robot design is unique in eldercare and is both the slimmest eldercare robot and the only one able to support the weight of a human far from

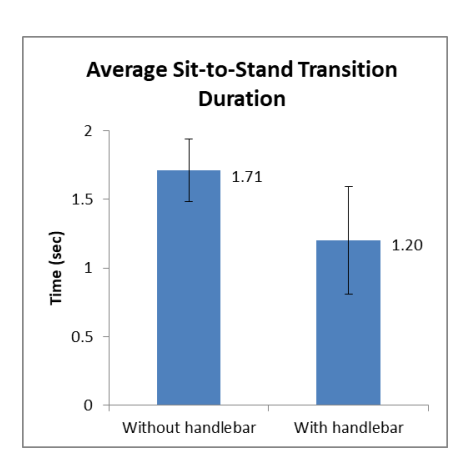


Fig. 10. The average duration for a sit-to-stand postural transition decreased by 29.77% with a frontal handlebar. The black bars represent the sample standard deviation. A one-tailed unequal variance (Welch) t test found the decrease to be significant relative to  $\alpha=0.05$ , with a p-value of 0.0042.

the base of the robot. We believe that its best use is to augment caretaker staff in nursing homes and assisted living communities. When elderly persons summon help to their rooms, the robot could be deployed for easier tasks such as postural assistance or sit-to-stand transfers. More challenging tasks or emergencies could be handled by a human, and the elderly persons would not have to worry about robot maintenance.

Future work involves fully exploiting the kinematic design of the robot to further improve trajectory following, conducting home trials with elderly persons, and adjusting the robot dimensions to better fit the home environment.

#### ACKNOWLEDGMENTS

This material is supported by the National Robotics Initiative Grant No. 2133072 and the National Science Foundation Graduate Research Fellowship under Grant No. 2141064. Human subject tests were reviewed and approved by the MIT Committee on the Use of Humans as Experimental Subjects (COUHES) under IRB number 2207000712.

## REFERENCES

- [1] "The US population is aging," Urban Institute, https://www.urban.org/policy-centers/cross-center-initiatives/program-retirement-policy/projects/data-warehouse/what-future-holds/us-population-aging (accessed Aug. 12, 2023).
- [2] Z. Caplan, "U.S. older population grew from 2010 to 2020 at fastest rate since 1880 to 1890," Census.gov, https://www.census.gov/library/stories/2023/05/2020-census-united-states-older-population-grew.html (accessed Aug. 12, 2023).
- [3] S. Marchese, "The Caregiver Shortage: Which States Are Doing Best," Asbestos.com, https://www.asbestos.com/support/caregivers/shortageby-state/ (Accessed Aug. 12, 2023).
- [4] A. Oldenburg, "Nationwide Caregiver Shortage Felt By Older Adults," Aarp.org, https://www.aarp.org/caregiving/basics/info-2022/in-home-caregiver-shortage.html (Accessed Aug. 12, 2023).
- [5] J. Biden, "Executive Order on Increasing Access to High-Quality Care and Supporting Caregivers," The White House, https://www.whitehouse.gov/briefing-room/presidential-actions/2023/04/18/executive-order-on-increasing-access-to-high-quality-care-and-supporting-caregivers/ (Accessed Aug. 12, 2023).
- [6] G. Bardaro, A. Antonini, and E. Motta, "Robots for Elderly Care in the Home: A Landscape Analysis and Co-Design Toolkit," in Int J of Soc Robotics 14, 657–681, Apr. 2022.

- [7] P. Asgharian, A. M. Panchea, and F. Ferland, "A Review on the Use of Mobile Service Robots in Elderly Care," in Robotics, vol. 11, no. 6, p. 127, Nov. 2022, doi: 10.3390/robotics11060127.
- [8] K. Barhydt and H. H. Asada, "A High-Strength, Highly-Flexible Robotic Strap for Harnessing, Lifting, and Transferring Humans," in IEEE Robotics and Automation Letters, vol. 8, no. 4, pp. 2110-2117, April 2023, doi: 10.1109/LRA.2023.3246389.
- [9] R. Agrigoroaie, F. Ferland, and A. Tapus, "The ENRICHME Project: Lessons Learnt from a First Interaction with the Elderly", in Social Robotics, 2016, pp. 735–745.
- [10] V. Pasqui, L. Saint-Bauzel, P. Rumeau, and N. Vigouroux, "Proposed Generic Method to Assess Efficiency of Smart-Walkers", in Impact Analysis of Solutions for Chronic Disease Prevention and Management, 2012, pp. 218–221.
- [11] R. Bolli, P. Bonato, and H. Asada, "A Handle Robot for Providing Bodily Support to Elderly Persons," 2023 IEEE/RSJ International Conference on Intelligent Robots and Systems (IROS), Detroit, USA, 2023.
- [12] I. Levine et al., "Grab Bar Use Influences Fall Hazard During Bathtub Exit," in Human factors, 187208211059860. 28 Dec. 2021.
- [13] A. W. Divelbiss and J. T. Wen, "A path space approach to non-holonomic motion planning in the presence of obstacles," in IEEE Transactions on Robotics and Automation, vol. 13, no. 3, pp. 443-451, June 1997.
- [14] R. Bolli and H. Asada, "A Data-Driven Approach to Positioning Grab Bars in the Sagittal Plane for Elderly Persons," Late-Breaking Report, 2023 32nd IEEE International Conference on Robot and Human Interactive Communication (RO-MAN), Busan, South Korea, 2023.
- [15] L. Axtell and Y. Yasuda, "Assistive Devices and Home Modifications in Geriatric Rehabilitation," in Clinics in Geriatric Medicine, 1993, 9(4), 803–821. doi:10.1016/s0749-0690(18)30378-1
- [16] H. Sveistrup et al., "Evaluation of Bath Grab Bar Placement for Older Adults," in Technology and Disability, 1 Jan. 2006: 45 – 55.
- [17] D. Johnson and J. Pauls, "Systemic stair step geometry defects, increased injuries, and public health plus regulatory responses," in Contemporary Ergonomics and Human Factors, 2010.
- [18] S. Chang et al, "Understanding stand-to-sit maneuver: implications for motor system neuroprostheses after paralysis," in Journal of rehabilitation research and development vol. 51,9, 2014
- [19] D. Biman and Y. Wang, "Isometric pull-push strengths in workspace: 1. Strength profiles," in International Journal of Occupational Safety and Ergonomics vol. 10,1, 2004
- [20] A. W. Divelbiss and J. T. Wen, "Trajectory tracking control of a cartrailer system," in IEEE Transactions on Control Systems Technology, vol. 5, no. 3, pp. 269-278, May 1997, doi: 10.1109/87.572125.
- [21] M. Islam, X. Ding and Y. He, "A closed-loop dynamic simulation-based design method for articulated heavy vehicles with active trailer steering systems", Vehicle System Dynamics, 2012
- [22] Y. Kanayama, Y. Kimura, F. Miyazaki and T. Noguchi, "A stable tracking control method for an autonomous mobile robot," Proceedings., IEEE International Conference on Robotics and Automation, Cincinnati, OH, USA, 1990, pp. 384-389 vol.1.
- [23] R. W. Brockett, "Asymptotic stability and feedback stabilization," Differential geometric control theory 27.1, 1983
- [24] J. Zabczyk, "Some comments on stabilizability," in Appl Math Optim 19, 1–9, 1989. https://doi.org/10.1007/BF01448189
- [25] R. Siegwart et al, "Introduction to Autonomous Mobile Robots, Second Edition," Intelligent robotics and autonomous agents, 2011.
- [26] M. Theers and M. Singh, "Pure Pursuit", Github, https://thomasfermi.github.io/Algorithms-for-Automated-Driving/Control/PurePursuit.html (Accessed Aug. 26, 2023)
- [27] L. Yi et al., "Multi-Objective Instantaneous Center of Rotation Optimization Using Sensors Feedback for Navigation in Self-Reconfigurable Pavement Sweeping Robot," Mathematics, vol. 10, no. 17, p. 3169, Sep. 2022, doi: 10.3390/math10173169.
- [28] Y. Shi, M. R. Elara, A. V. Le, V. Prabakaran and K. L. Wood, "Path Tracking Control of Self-Reconfigurable Robot hTetro With Four Differential Drive Units," in IEEE Robotics and Automation Letters, vol. 5, no. 3, pp. 3998-4005, July 2020, doi: 10.1109/LRA.2020.2983683.
- [29] H. Jin and M. Zhou, "On the road friction recognition based on the driving wheels deceleration," 2014 IEEE Conference and Expo Transportation Electrification Asia-Pacific (ITEC Asia-Pacific), Beijing, China, 2014, pp. 1-8, doi: 10.1109/ITEC-AP.2014.6940633.